Copper Complexes Hot Paper

Deutsche Ausgabe: DOI: 10.1002/ange.201607238
Internationale Ausgabe: DOI: 10.1002/anie.201607238

Characterization and Reactivity Studies of a Terminal Copper–Nitrene Species

Teresa Corona, Lídia Ribas, Mireia Rovira, Erik R. Farquhar, Xavi Ribas, Kallol Ray,* and Anna Company**

Abstract: *High-valent terminal copper–nitrene species have been postulated as key intermediates in copper-catalyzed aziridination and amination reactions. The high reactivity of these intermediates has prevented their characterization for decades, thereby making the mechanisms ambiguous. Very recently, the Lewis acid adduct of a copper–nitrene intermediate was trapped at −90 °C and shown to be active in various oxidation reactions. Herein, we describe for the first time the synthesis and spectroscopic characterization of a terminal copper(II)–nitrene radical species that is stable at room temperature in the absence of any Lewis acid. The azide derivative of a triazamacrocyclic ligand that had previously been utilized in the stabilization of aryl–Cu^{III} intermediates was employed as an ancillary ligand in the study. The terminal copper(II)–nitrene radical species is able to transfer a nitrene moiety to phosphines and abstract a hydrogen atom from weak C–H bonds, leading to the formation of oxidized products in modest yields.*

Terminal high-valent copper–nitrene intermediates have long been proposed as key intermediates in aziridination and amination reactions.[1–3] Obtaining mechanistic insight into these transformations and developing selective catalytic reagents and processes are only possible if the structure and properties of these key species are fully understood. Whereas metal–nitrene species based on iron, cobalt, and nickel have been isolated,[4–9] terminal copper–nitrene intermediates have eluded detection for decades. Warren and co-workers indirectly proposed the involvement of terminal copper–nitrene intermediates derived from dicopper–nitrene species by NMR exchange experiments and kinetic measurements of C–H functionalization reactions.[2,10] More recently, the involvement of such species in copper-mediated oxidation reactions was corroborated by the spectroscopic trapping of Lewis acid adducts of a copper–nitrene intermediate at −90 °C.[11,12] Furthermore, Bertrand and co-workers recently reported isolated examples of copper(II)–bis(nitrene) and dicopper(II)–nitrene species that were obtained by reacting a bulky phosphinonitrene ligand with 0.5 and 2 equiv of copper(I) triflate, respectively. However, terminal copper–nitrene intermediates could not be isolated in these reactions although their formation was suggested based on ^{31}P NMR studies.[13] Herein, we report the unprecedented spectroscopic and theoretical characterization of terminal copper–nitrene species (**1** and **3**) in the absence of any Lewis acid by employing azide derivatives of triazamacrocyclic ligands (^{H}L-N_3 and ^{Me}L-N_3). Such ligand architectures have previously been utilized in the successful stabilization of aryl–Cu^{III} intermediates by enforcing a square-planar geometry at the copper center.[14,15] Moreover, copper–nitrene species **3**, which is stable at room temperature, participates in a number of nitrene transfer and C–H activation reactions, thus providing a key precedent for the possible involvement of such species in oxidation catalysis.

While some of us studied the relevance of aryl–Cu^{III} species in model copper-catalyzed C_{aryl}–C_{sp^3},[16] C_{aryl}–C_{sp},[17] and C_{aryl}–heteroatom[14,15,18,19] bond-formation reactions, we envisaged that compound ^{H}L-N_3 (Scheme 1) could be a good candidate as a starting material for the preparation of elusive copper–nitrene complexes (see the Supporting Information

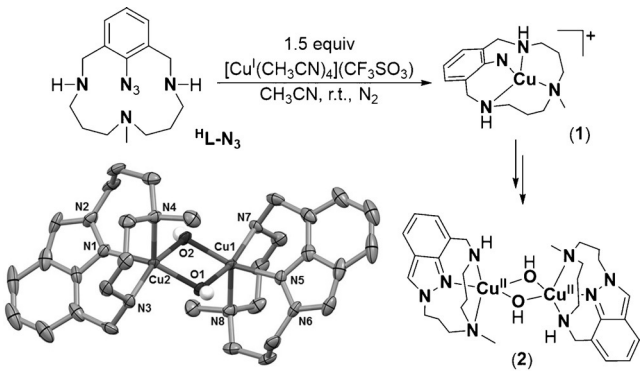

Scheme 1. Schematic representations of **1** and **2**. X-ray structure of **2**. Thermal ellipsoids set at 50% probability. Hydrogen atoms (except for those belonging to the OH groups) and triflate anions omitted for clarity.

[*] T. Corona, L. Ribas, M. Rovira, Dr. X. Ribas, Dr. A. Company
Grup de Química Bioinspirada, Supramolecular i Catàlisi (QBIS-CAT)
Institut de Química Computacional i Catàlisi (IQCC)
Departament de Química, Universitat de Girona
Campus Montilivi, E17003 Girona, Catalonia (Spain)
E-mail: xavi.ribas@udg.edu
anna.company@udg.edu
Dr. E. R. Farquhar
Case Western Reserve University Center for Synchrotron Biosciences and Center for Proteomics and Bioinformatics
National Synchrotron Light Source II
Brookhaven National Laboratory, Upton, New York 11973 (USA)
Prof. Dr. K. Ray
Department of Chemistry
Humboldt Universität zu Berlin
Brook-Taylor Strasse 2, 12489 Berlin (Germany)
E-mail: kallol.ray@chemie.hu-berlin.de
Supporting information and the ORCID identification number(s) for the author(s) of this article can be found under: http://dx.doi.org/10.1002/anie.201607238.

for its synthesis). Accordingly, the reaction of ^{H}L-N$_3$ with 1.5 equiv [Cu^{I}(CH$_3$CN)$_4$](CF$_3$SO$_3$) in acetonitrile at room temperature under argon atmosphere was monitored by UV/Vis spectroscopy (see the Supporting Information, Figure S3). The formation of a green transient species (**1**, $\lambda_{max} = 380$ and 790 nm) was observed during the first stages of the reaction. However, this compound quickly evolved into a purple species (**2**, $\lambda_{max} = 550$ nm, $\varepsilon = 1000\,M^{-1}cm^{-1}$), which proved to be stable for several hours at room temperature. Violet crystals (isolated in 56% yield) were obtained by slow diethyl ether diffusion into an acetonitrile solution of **2** at −30 °C.

The X-ray structure of **2** reveals a dimeric core with significant modification of the initial ^{H}L-N$_3$ structure (Scheme 1). Loss of a N$_2$ molecule from the azide unit is accompanied by N−N bond formation, giving rise to the formation of an indazole ring. Each Cu center adopts a distorted square-pyramidal geometry ($\tau = 0.1$)[20] and binds to the N−CH$_3$, NH, and N$_{aryl}$ groups of the resulting indazole-based ligand (L^{in}) as well as to two additional hydroxo ligands, thereby forming a bis(μ-hydroxo)dicopper(II) core in **2** (Scheme 1). The hydroxo groups in **2** presumably originate from adventitious water present in the anhydrous solvents used in the glovebox;[21] they also enforce a strong antiferromagnetic coupling between the two copper centers, which results in an $S = 0$ ground state.[22] The integrity of this dimeric structure in solution was confirmed by ^{1}H NMR studies, which showed a diamagnetic spectrum in which the indazole protons could be clearly observed at 8.2, 7.7, 7.2, and 7.1 ppm (Figure S4). Although unknown in copper chemistry, the N−N bond-formation reaction associated with the formation of **2** is typically exhibited by high-valent terminal metal–imido or –nitrido complexes.[5,23–25] A similar terminal copper–nitrene intermediate could also play a key role during the copper-mediated N−N bond-formation reaction that leads to the formation of **2**.

Whereas UV/Vis studies clearly confirmed the presence of a transient intermediate (**1**) along the reaction of ^{H}L-N$_3$ with Cu^{I} at 25 °C to form **2**, spectroscopic assignment of the electronic structure of **1** proved to be difficult because of its instability at 25 °C. However, the stability of **1** could be significantly increased by generating it in acetone at −50 °C (λ_{max} [ε, $M^{-1}cm^{-1}$] = 380 [>1300], 650 [>150], and 790 nm [>200]; Figure S7). Notably, cold spray ionization mass spectrometry (CSI-MS) of **1** (Figure S8) gave rise to a major peak centered at *m*/*z* 323.1284 with a mass and isotope distribution pattern consistent with a terminal copper–nitrene species [Cu(^{H}L-N)]$^+$, where ^{H}L-N is the ligand formed after N$_2$ release from ^{H}L-N$_3$. The low temperatures required to prevent the decomposition of **1** into **2**, however, prevented us from investigating the oxidizing capability of **1**.

To increase the thermal stability of the putative copper–nitrene intermediate, efforts were made to block the facile decomposition of **1** into **2** by introducing methyl groups in the secondary amine units of the ^{H}L-N$_3$ ligand (see the Supporting Information for synthetic procedures). UV/Vis monitoring of the stoichiometric reaction between the methylated version of the azide-derived ligand (^{Me}L-N$_3$, Scheme 2) and [Cu^{I}(CH$_3$CN)$_4$](CF$_3$SO$_3$) in acetonitrile at 25 °C showed the formation of a stable green species (**3**; $t_{1/2} \approx 45$ h) with

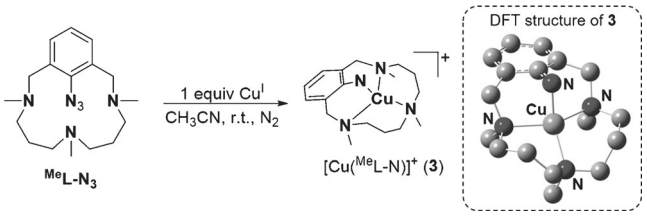

Scheme 2. Schematic representation of **3** together with its DFT optimized structure.

a distinct absorption spectrum (λ_{max} [ε, $M^{-1}cm^{-1}$] = 360 [>1200], 710 nm [>200], and 980 nm [>150]; Figure 1a) relative to **1**.[26] CSI-MS analysis revealed a dominant peak at *m*/*z* 351.1597 with a mass and isotope pattern fully consistent with [Cu(^{Me}L-N)]$^+$, which was partially shifted to *m*/*z* 352.1601 when 50% ^{15}N-labeled **3**[27] was used (Figure 1b). Moreover, the EPR spectrum of **3** only exhibited a small signal of Cu^{II}, which accounted for less than 5% of the sample; the majority of the species present in solution were not detectable by X-band EPR spectroscopy. Importantly, FTIR analysis of a concentrated solution of **3** did not exhibit any azide vibration at about 2200 cm^{-1}, further confirming N$_2$ release in line with the MS experiments. Furthermore, a low-intensity band at 426 cm^{-1} could be observed in the IR spectrum, which was attributed to a Cu–N vibration based on

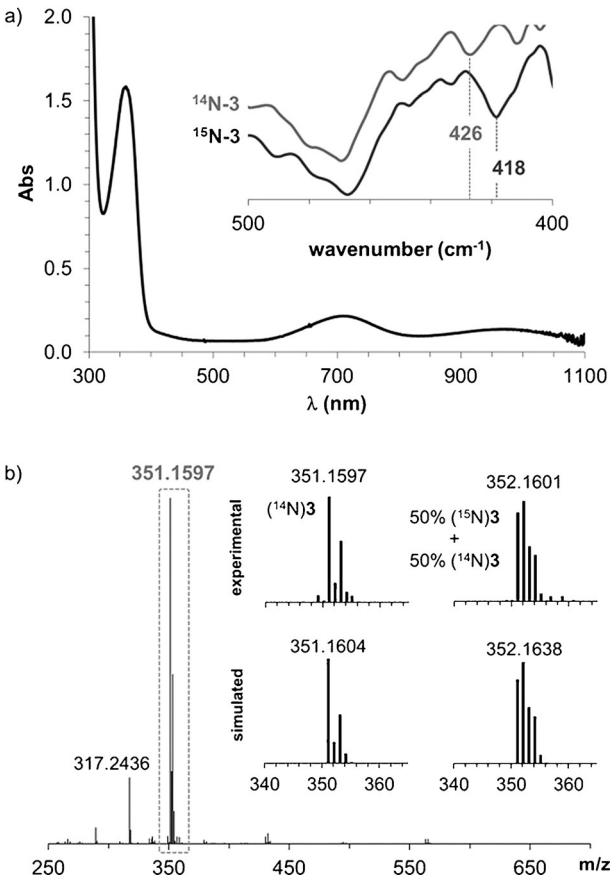

Figure 1. a) UV/Vis spectrum of **3** in acetonitrile at 25 °C. Inset: FTIR spectrum of **3** (gray) and its 50% ^{15}N-labeled analogue (black). b) ESI-MS spectrum of **3** in acetonitrile at 25 °C under N$_2$ atmosphere.

the $^{15}N/^{14}N$ downshift of 8 cm^{-1} upon ^{15}N labeling (Figure 1a, inset). Finally, an effective magnetic moment (μ_{eff}) of 2.14 μ_B, as determined by the Evans' method,[28,29] confirmed the $S=1$ ground state of **3**. Note that the μ_{eff} of **3** is significantly lower than expected for the spin-only value of a typical $S=1$ system ($\mu_{eff}=2.83\ \mu_B$); this can be attributed to the presence of unreacted copper(I) or copper(II) impurities in solutions of **3**.

We then turned to X-ray absorption spectroscopy (XAS) to directly probe the oxidation state of copper in **3**. Notably, **3** exhibited X-ray absorption near-edge structure (XANES) features nearly identical to those of the dinuclear Cu^{II} complex **2**. This finding strongly suggests that **3** also contains a Cu^{II} center (Figure S9); together with the experimentally determined μ_{eff} value of 2.14 μ_B, this may indicate an $[Cu^{II}(^{Me}L\text{-}N^{\bullet-})]^+$ electronic structure for **3**. Extended X-ray absorption fine structure (EXAFS) analysis revealed further structural details. For **3**, the first coordination sphere could be satisfactorily fitted by four nitrogen scatterers at a distance of 2.04 Å (Table S3, Figure S10). The outer-shell features could be accounted for by single scattering paths arising from two carbon atoms at 2.44 Å and twelve carbon atoms at 3.23 Å. EXAFS analysis of **2** was also performed to determine whether the solid-state dimeric structure is retained in a frozen acetonitrile solution. The best fit (Table S4) of the Cu EXAFS data of **2** consists of two subshells of four short N/O scatterers at 1.99 Å and one long N/O scatterer at 2.13 Å, supporting a five-coordinate Cu center in **2**, which is in agreement with the XRD studies (see above). Fits to a single shell of 5–6 nitrogen scatterers produced a significant decrease in fit quality. Cu EXAFS analysis of **2** also showed a shell at 2.93 Å corresponding to the Cu scatterer, which is in reasonable agreement with the Cu–Cu distance of 3.03 Å determined by XRD.

DFT calculations at the B3LYP/TZVP level of theory in acetonitrile at 298 K predicted a triplet ($S=1$; $J=+3.2\ cm^{-1}$) ground state for **3**. The excited open- and closed-shell singlet electronic states were determined to be 3 and 18 kcal mol^{-1} higher in energy, respectively. The copper center in the calculated structure of **3** (Scheme 2) adopts a strongly distorted tetrahedral geometry involving coordination of the four nitrogen atoms of ^{Me}L-N. Notably, the calculated metrical parameters are in reasonable agreement with the experimentally determined values (Table S3). Furthermore, the theoretically predicted Cu–N_{aryl} vibration at 427 cm^{-1} with a −6 cm^{-1} shift upon ^{15}N labeling is fully congruent with the experimental IR spectrum (see above). Interestingly, a spin density of 1.20 was obtained for the N_{aryl} atom, indicating that the excess unpaired electron density on nitrogen is larger than expected for a classical metal–nitrene radical system (Figures S18 and S19). Such a non-classical electronic structure has been reported previously for a cobalt–oxo species[30] and may be understood by considering the contribution of the Cu^{I}–nitrene biradical resonance form, where two electrons from the N_{aryl} atom moiety are transferred to the Cu center. The calculated spin density of 0.4 on the copper atom, which is significantly lower than the expected value of 1 for a Cu^{II} center, further confirms the contribution of both $[Cu^{II}(^{Me}L\text{-}N^{\bullet-})]^+$ and $[Cu^{I}(^{Me}L\text{-}N^{\bullet})]^+$ resonance forms to the electronic structure of **3**.

The reactivity of **3** in various oxidation reactions was also investigated. For example, transfer of the ^{Me}L-N unit of the copper–nitrene species **3** to phosphines was evaluated. The green color of a solution of **3** in acetonitrile disappeared upon addition of triphenylphosphine (PPh_3). ESI-MS analysis of the final reaction mixture gave rise to a peak at m/z 551.35, which is consistent with nitrogen insertion to the phosphorus atom to form ^{Me}L-N=PPh_3; this peak was shifted by one mass unit when 50% ^{15}N-labeled **3** (Figure S13) was used in the reaction. ^{31}P NMR analysis showed the presence of a resonance at 25.6 ppm, which falls in the region typical for N=P bonds,[31] that accounted for a yield of 41% with respect to **3** (NMR quantification using $OPPh_3$ as an internal standard). Interestingly, ^{31}P NMR analysis of a sample prepared by reacting 50% ^{15}N-labeled **3** with PPh_3 afforded the peak at 25.6 ppm together with a doublet at 25.3 ppm, corresponding to ^{Me}L-^{15}N=PPh_3, where coupling of ^{31}P with ^{15}N ($S=1/2$) occurs (Figure S14). The measured coupling constant of $J_{N,P}=38.2$ Hz is in accordance with those typically measured for N–P bonds, further supporting the formation of the nitrene transfer product.[32] UV/Vis monitoring of this reaction using excess substrate showed that the decay of the bands at 710 and 980 nm, which are associated with **3**, followed a pseudo-first-order behavior, so that the kinetic traces could be fitted with single exponentials (Figure S12). The observed reaction rate (k_{obs}) was in turn found to be linearly dependent on the substrate concentration, affording a second order constant (k_2) of 7.5 $M^{-1}s^{-1}$ for the reaction with PPh_3. Interestingly, the k_2 values were highly dependent on the substituents at the phosphorus atom. Thus the reaction of **3** with sterically bulkier tri(*o*-tolyl)phosphine was two orders of magnitude slower (0.052 $M^{-1}s^{-1}$) than that with PPh_3 whereas the reaction with tri(*n*-butyl)phosphine was too fast, and the reaction rate could not be determined. Finally, the reaction rates were found to be dependent on the substituent at the *para* position of the aryl groups attached to the phosphine. The logarithm of the second-order rate constants of a series of *para*-X-triarylphosphine (X = Me, H, and Cl) derivatives gave a negative correlation with the Hammett parameter (σ_p) with a reaction constant (ρ) of −1.9, which is indicative of the electrophilic character of **3** (Figure S15).

Reactions of **3** with hydrocarbons bearing C–H bonds with low dissociation energies (BDEs) were also evaluated, and xanthene was used as a model substrate. Strikingly, the k_2 value measured for this reaction ($k_2=0.009\ M^{-1}s^{-1}$, BDE = 75.5 kcal mol^{-1}) was lower than that determined for the reaction with 1,4-cyclohexadiene ($k_2=0.020\ M^{-1}s^{-1}$, BDE = 78 kcal mol^{-1}), which does not correlate with the C–H bond strength. Again, steric hindrance could be a reason for this result so that the smaller 1,4-cyclohexadiene substrate reacts faster despite its increased C–H bond strength (Table S5). Furthermore, a kinetic isotope effect of 5.2 was measured when $[D_2]$xanthene was used as the substrate at 25 °C (Figure S16).

In summary, we have reported the synthesis and spectroscopic characterization of a terminal copper–nitrene species (**3**) without the need of using redox-innocent cations such as Sc^{3+}. The apparently simple methylation of the secondary amines in ^{H}L-N_3 was crucial to slow down the N–N bond-

formation event, thus retarding the main decomposition pathway for the copper–nitrene species in this system. Interestingly, this species could be trapped at room temperature, and it can undergo nitrogen-transfer reactions to organic substrates such as phosphines and abstract hydrogen atoms from weak C–H bonds.

Acknowledgements

This work was supported by the European Commission (2011-CIG-303522 to A.C.), the MINECO of Spain ("Ramón y Cajal" contract to A.C. and CTQ2013-43012-P to A.C. and X.R.), the Clara Immerwahr award of UniCat (to A.C.), the European Research Council (Starting Grant ERC-2011-StG-277801 to X.R.), and the Generalitat de Catalunya (2014 SGR 862). K.R. thanks the DFG for a Heisenberg Professorship. X.R. also acknowledges an ICREA Acadèmia award. The XAS measurements at SSRL BL 2-2 were made possible by the US Department of Energy, Office of Science (DE-AC02-76SF00515 and DE-SC0012704 to SSRL and NSLS-II, respectively) and the US National Institutes of Health (P30-EB-009998 to the CWRU Center for Synchrotron Biosciences).

Keywords: copper–nitrene species · density functional calculations · hydrogen atom abstraction · mass spectrometry · nitrene transfer

How to cite: *Angew. Chem. Int. Ed.* **2016**, *55*, 14005–14008
Angew. Chem. **2016**, *128*, 14211–14214

[1] R. T. Gephart, T. H. Warren, *Organometallics* **2012**, *31*, 7728–7752.
[2] Y. M. Badiei, A. Krishnaswamy, M. M. Melzer, T. H. Warren, *J. Am. Chem. Soc.* **2006**, *128*, 15056–15057.
[3] Y. M. Badiei, A. Dinescu, X. Dai, R. M. Palomino, F. W. Heinemann, T. R. Cundari, T. H. Warren, *Angew. Chem. Int. Ed.* **2008**, *47*, 9961–9964; *Angew. Chem.* **2008**, *120*, 10109–10112.
[4] K. Ray, F. Heims, F. F. Pfaff, *Eur. J. Inorg. Chem.* **2013**, 3784–3807.
[5] J. Hohenberger, K. Ray, K. Meyer, *Nat.Commun.* **2012**, *3*, 720.
[6] X. Hu, K. Meyer, *J. Am. Chem. Soc.* **2004**, *126*, 16322–16323.
[7] D. A. Iovan, T. A. Betley, *J. Am. Chem. Soc.* **2016**, *138*, 1983–1993.
[8] C. A. Laskowski, A. J. M. Miller, G. L. Hillhouse, T. R. Cundari, *J. Am. Chem. Soc.* **2011**, *133*, 771–773.
[9] L. Zhang, Y. Liu, L. Deng, *J. Am. Chem. Soc.* **2014**, *136*, 15525–15528.
[10] M. J. B. Aguila, Y. M. Badiei, T. H. Warren, *J. Am. Chem. Soc.* **2013**, *135*, 9399–9406.
[11] S. Kundu, E. Miceli, E. Farquhar, F. F. Pfaff, U. Kuhlmann, P. Hildebrandt, B. Braun, C. Greco, K. Ray, *J. Am. Chem. Soc.* **2012**, *134*, 14710–14713.
[12] I. Monte-Pérez, S. Kundu, K. Ray, *Z. Anorg. Allg. Chem.* **2015**, *641*, 78–82.
[13] F. Dielmann, D. M. Andrada, G. Frenking, G. Bertrand, *J. Am. Chem. Soc.* **2014**, *136*, 3800–3802.
[14] A. Casitas, M. Canta, M. Solà, M. Costas, X. Ribas, *J. Am. Chem. Soc.* **2011**, *133*, 19386–19392.
[15] A. Casitas, A. E. King, T. Parella, M. Costas, S. S. Stahl, X. Ribas, *Chem. Sci.* **2010**, *1*, 326–330.
[16] M. Rovira, M. Font, X. Ribas, *ChemCatChem* **2013**, *5*, 687–691.
[17] M. Rovira, M. Font, F. Acuña-Parés, T. Parella, J. M. Luis, J. Lloret-Fillol, X. Ribas, *Chem. Eur. J.* **2014**, *20*, 10005–10010.
[18] L. M. Huffman, A. Casitas, M. Font, M. Canta, M. Costas, X. Ribas, S. S. Stahl, *Chem. Eur. J.* **2011**, *17*, 10643–10650.
[19] M. Font, T. Parella, M. Costas, X. Ribas, *Organometallics* **2012**, *31*, 7976–7982.
[20] D. S. Marlin, M. M. Olmstead, P. K. Mascharak, *Inorg. Chem.* **2001**, *40*, 7003–7008.
[21] The hydroxo ligands in the structure of **2** were found to undergo exchange with $H_2{}^{18}O$, as determined by ESI-MS (see Figure S6).
[22] M. Costas, X. Ribas, A. Poater, J. M. López Valbuena, R. Xifra, A. Company, M. Duran, M. Solà, A. Llobet, M. Corbella, M. A. Usón, J. Mahía, X. Solans, X. Shan, J. Benet-Buchholz, *Inorg. Chem.* **2006**, *45*, 3569–3581.
[23] T. A. Betley, J. C. Peters, *J. Am. Chem. Soc.* **2004**, *126*, 6252–6254.
[24] K. C. MacLeod, D. J. Vinyard, P. L. Holland, *J. Am. Chem. Soc.* **2014**, *136*, 10226–10229.
[25] N. D. Harrold, R. Waterman, G. L. Hillhouse, T. R. Cundari, *J. Am. Chem. Soc.* **2009**, *131*, 12872–12873.
[26] Analogously to **1**, self-decomposition of **3** occurred by N_2 release and N–N bond formation to form an indazole ring (70% yield) along with methane release (see the Supporting Information).
[27] 50% ^{15}N-labeled **3** was formed by reaction of $[Cu^{I}(CH_3CN)_4](CF_3SO_3)$ with singly ^{15}N-labeled ^{Me}L-N_3 (synthesized by reaction of ^{Me}L-Br with singly terminal-labeled sodium azide).
[28] D. F. Evans, *J. Chem. Soc.* **1959**, 2003–2005.
[29] M. L. Naklicki, C. A. White, L. L. Plante, C. E. B. Evans, R. J. Crutchley, *Inorg. Chem.* **1998**, *37*, 1880–1885.
[30] D. W. Crandell, S. Ghosh, C. P. Berlinguette, M.-H. Baik, *ChemSusChem* **2015**, *8*, 844–852.
[31] S. Kundu, PhD Thesis, Department of Chemistry, Humboldt Universität zu Berlin (Germany), **2013**.
[32] W. Gombler, R. W. Kinas, W. J. Stec, *Z. Naturforsch* **1983**, *38*, 815–818.

Received: July 26, 2016
Published online: October 10, 2016

